ORIGINAL ARTICLE

DEM-FEM coupling simulation of residual stresses and surface roughness induced by shot peening of TC4 titanium alloy

Kaifa Li[1] · Cheng Wang[1] · Xingyuan Hu[1] · Yijun Zhou[1] · Yongbin Lai[1] · Chuanli Wang[1,2]

Abstract

An integrated DEM-FEM coupling simulation approach is developed to simulate the real process of shot peening, and is validated by comparing the predicted in-depth residual stresses with the experimentally measured results. Two kinds of three-dimensional finite element models associated with the original surface roughness of $R_{a0} = 26.7\mu m$ and $50.1\mu m$ are respectively established by using Gaussian distribution in conjunction with the exponential autocorrelation function, and another target model without the original surface roughness is utilized for reference purposes. Taking advantage of the integrated DEM-FEM coupling simulations of shot peening processes based on the three kinds of target models, the effects of the original surface roughness, shot impact angle, and shot peening coverage on the shot-peened residual stresses and surface roughness are investigated in detail. The obtained results show that the larger original surface roughness of TC4 titanium alloy could be reduced by shot peening, and the reduction increases with the increasing shot peening coverage from 100 to 200%. In the target models associated with the original surface roughness, the distributions of shot-peened surface residual stresses tend to be more uniform than that in the target model without the original surface roughness, whereas both the in-depth residual stresses and surface roughness are not very sensitive to the changes of shot impact angle in the range from 60° to 90°.

Keywords Shot peening · DEM-FEM coupling simulation · Residual stresses · Surface roughness · TC4 titanium alloy · Numerical simulation

1 Introduction

Shot peening is acknowledged as an effective mechanical cold-working technique for surface strengthening of the metallic materials, and is constantly and widely utilized in the aerospace and aircraft industry for improving the fatigue performance of titanium alloy components [1–4]. During the process of the conventional shot peening, a large number of shots are driven to impact on the ductile metallic surface to be treating by the gas pressure or the rotational centrifugal force, and the shot velocity is usually in the range from 20 to 150 m/s. As a result of the multiple shot impacts, the significant elastic-plastic deformations are produced in the shot-peened surface and subsurface layers. As the recovery of the elastic deformation region is constrained by the irrecoverable plastic deformation region, the beneficial compressive residual stresses in the shot-peened surface and subsurface layers are produced resultantly, which are responsible for the improvement of fatigue resistance of the shot-peened materials [5–8]. However, on the other hand, the surface roughness caused by shot peening is generally considered to be unfavorable for the surface integrity of the shot-peened metallic components; the larger surface roughness could increase the stress concentration and promote the microcracks initiation and propagation rapidly at the surface geometrical defects, resulting in the dramatic reduction of fatigue life [9, 10]. It is generally regarded as the competitive relation between the compressive residual stresses and surface roughness for the shot-peened metallic materials [11–13].

There are a considerable number of factors influencing the shot-peened residual stresses and surface roughness, such as the shot size, shot mass density, shot impact velocity, shot

✉ Cheng Wang
aust_wangch@163.com

1 School of Mechanical Engineering, Anhui University of Science and Technology, Huainan 232001, China

2 Anhui Key Laboratory of Mine Intelligent Equipment and Technology, Anhui University of Science and Technology, Huainan 232001, China

impact angles and mass flow speed, etc. [14–16]. It should be noted that the different selections of shot peening process parameters could obtain an approximately identical shot-peened results. In order to reproduce, compare, and control shot peening processes, two quality parameters involving shot peening coverage and intensity are extensively used in industry [17, 18]. Shot peening coverage is the percentage of the dented surface on the target surface to be peening, as defined by SAE J2277 standard (2013). The shot peening intensity is characterized by the arc heights of Almen samples, and the saturation point is defined as the deflection of the arc height at which doubling the peening time increases its value by 10%.

By using the shot peening coverage and Almen intensity, a large number of experiments have been performed to investigate the strengthening mechanism of shot peenning and optimize the shot peening process parameters so far [19–22]. The experimentally measured residual stresses, surface hardness, and surface roughness are usually used to evaluate the strengthening effects of shot peening [23–26]. However, it is too costly and time-consuming to carry out the experimental studies of shot peening for so many metallic materials, in particular the different shot peening conditions are taken into consideration. With the development of computer technology and finite element method, the numerical simulations of shot peening have emerged and attracted a great deal of interest [27–30]. Compared with the experiment study, the numerical simulations not only have the advantages of economical cost and time saving, but also provide valuable insight into the correlation between the residual stresses (or surface roughness) and the shot peening process parameters [31, 32]. In general, the developed finite element models of shot peening have been validated by the experimental results in terms of the residual stresses, surface hardness, and surface roughness [33–36].

A significant amount of effort has been done by the researchers all over the world to develop the finite element models of shot peening for the numerical study. As well known, the two-dimensional axis-symmetric model is widely used to simulate the process of single shot impact owing to its simplicity, and the elastic-plastic deformation resulting from the interaction between the single shot and metallic surface can be quantitatively studied [37]. Due to the incapability of simulating the processes of multiple shot impacts for the axis-symmetric model, the three-dimensional finite element models of shot peening have been developed, which can be approximately divided into two categories: the prior positioning shots [38, 39] and random positioning shots [40–42]. For the first category with respect to the prior positioning shots, the well-known symmetric cell model [43, 44] has been proved to be able to predict the residual stresses induced by shot peening, but the surface roughness caused by shot peening cannot be studied quantificationally, which is related to the random impacts of multiple shots. On the other hand,

the other category of shot peening models associated with the random positioning shots has the capability of reproducing the shot-peened surface topographies, and the surface roughness can be calculated accordingly [45–47]. However, the major drawback of the second category of shot peening models is that the shot-shot interaction is not taken into consideration.

In order to simulate the real process of shot peening as more as possible, the discrete element method (DEM) has been employed to compute the movement behaviors of the multiple shots, and the data on the impact velocities and positions of the multiple shots is then transferred to the three-dimensional finite element models of shot peening, the alternative approach coupling discrete element method with finite element method (DEM-FEM) is developed resultantly [48–50]. In the DEM-FEM coupling simulation of shot peening process, both the shot-shot interaction and shot-target interaction are taken into account; the residual stresses and surface roughness induced by shot peening can be predicted more correctly, and some complex shot peening phenomena could even be reproduced.

According to the literatures on the numerical simulations of shot peening process, the DEM-FEM coupling simulation approach has been becoming more and more popular in the numerical simulations of shot peening process in recent years. Hong et al. [51] presented the computational modeling of shot peening process by coupling DEM-FEM very earlier, and the interaction between incoming shots and rebounding shots are taken into account. Jebahi et al. [52] developed a new discrete-continuum coupling model and a comprehensive methodology for numerical simulation of shot peening at minimal cost. Tu et al. [53] proposed a sequential coupled discrete element-periodic cell-based finite element model to predict the shot-peened residual stresses and surface roughness, and the predicted results are comparable to the experimentally measured values. Zhang et al. [54] predicted the shot peening coverage, compressive residual stress, and surface roughness by the DEM-FEM coupling simulation method. Ahmad et al. [55] developed the DEM-FEM coupling model for the numerical simulation of the shot peening process with multiple random shots; the shot peening model was validated by experiments and was used to evaluate the effects of shot velocity, shot size, and impact angle on the resultant residual stresses. Marini et al. [56] explored the potentiality of DEM-FEM to simulate the shot peening on an edge, and the predicted residual stress field is in reasonable agreement with the reconstructed residual stress field based on experimental measurements.

In the majority of the developed finite element models of shot peening, including the DEM-FEM coupled models as stated above, the surface to be peening was generally treated as a plane; in other words, the effect of the original surface roughness was not taken into consideration. According to the experiment and simulation results, under the same shot peening condition, the shot-peened surface roughness would

increase and tend to be stable with the increase of shot peening coverage. However, it has seldom been reported on what it would become after shot peening of the metallic materials surface with the larger original surface roughness. Therefore, in order to investigate the effect of the original surface roughness on the shot-peened results, the Gaussian distribution in conjunction with the exponential autocorrelation function was used to modeling the original rough surface to be peening as described in the following section. Additionally, an integrated DEM-FEM coupling simulation approach of shot peening is developed and validated in the Section 2. The effects of the original surface roughness, shot impact angle, and shot peening coverage are investigated and discussed in the Section 3. Section 4 presents some conclusions at the end of this paper. Considering that TC4 titanium alloy is widely used in the aerospace and aircraft industry owing to its high strength, high corrosion resistance, and light weight, TC4 titanium alloy is therefore used as the metallic material to be peening in this work.

2 DEM-FEM coupling simulation and validation

2.1 Modeling of the original rough surface

Taking into account the effect of the original surface roughness on the shot-peened residual stresses and surface roughness, the original rough surface was numerically modeled by taking advantage of the Gaussian distribution in conjunction with the exponential autocorrelation function.

Firstly, a two-dimensional random sequence of white noise following Gaussian distribution, $\eta(x, y)$, is generated by using the computer, and is further converted into $A(\omega_x, \omega_y)$ through Fourier transform, wherein x and y represent the two-dimensional coordinates and ω_x and ω_y are the converted variables corresponding to x and y in $\eta(x, y)$.

Secondly, the exponential autocorrelation function, $R(\tau_x, \tau_y)$, is developed and expressed as

$$R(\tau_x, \tau_y) = \chi^2 \exp\left[-2.3\sqrt{\left(\frac{\tau_x}{\beta_x}\right)^2 \times \left(\frac{\tau_y}{\beta_y}\right)^2}\right] \quad (1)$$

where τ_x and τ_y represent the time delay, χ represents the surface RMS (root mean square) roughness, and β_x and β_y represent the correlation lengths along the x and y directions, respectively.

Thirdly, the power spectral density function (PSDF), $G_z(\omega_x, \omega_y)$, is obtained by Fourier transform on $R(\tau_x, \tau_y)$.

Fourthly, according to the following Eq. (2) [57], the transfer function of the filter, $H(\omega_x, \omega_y)$, can be obtained, i.e.,

$$H(\omega_x, \omega_y) = \sqrt{\frac{G_z(\omega_x, \omega_y)}{C_z}} \quad (2)$$

where C_z is a constant.

Fifthly, by multiplying $H(\omega_x, \omega_y)$ with $A(\omega_x, \omega_y)$, the Fourier transformation of the output sequence, $Z(\omega_x, \omega_y)$, with respect to the input sequence, $\eta(x, y)$, is calculated by

$$Z(\omega_x, \omega_y) = H(\omega_x, \omega_y) \cdot A(\omega_x, \omega_y) \quad (3)$$

Lastly, the height distribution function of the original rough surface, $z(x, y)$, can be directly obtained with the inverse Fourier transformation of $Z(\omega_x, \omega_y)$.

A routine was written in MATLAB to create the original rough surface according to Eqs. (1–3), as shown in Fig. 1; the peak height or wave depth of the rough surface can be effectively adjusted by introducing a coefficient k_z to multiply with $z(x, y)$. The node coordinate information outputted from MATLAB was imported into the three-dimensional drawing software Pro/Engineer (Pro/E), and the target models associated with the original surface roughness were resultantly created and shown in Fig. 1.

Two kinds of target models with the given original surface roughness resulting from the rough machining, $R_{a0} = 26.7\mu m$ and 50.1 μm which respectively corresponds to $R_{q0} = 31.6\mu m$ and 6μm, were created to investigate the effect of the original surface roughness on the shot-peened residual stresses and surface roughness. The symbols of R_a and R_q respectively denote the arithmetic average and the root-mean-square deviation of the three-dimensional surface roughness, which are expressed as

$$R_a = \frac{1}{N_s} \sum_{i=1}^{N_s} |Z_i| \quad (4)$$

$$R_q = \sqrt{\frac{1}{N_s} \sum_{i=1}^{N_s} Z_i^2} \quad (5)$$

where Z_i represents the distance of the nodes from the reference plane and N_s represents the number of nodes within the reference area. The target model without the original surface roughness was utilized for reference purposes and was represented as $R_{a0} = 0$ μm or $R_{q0} = 0$μm. The three kinds of target models associated with the different original surface roughness were imported into ABAQUS/CAE for meshing from Pro/E, as shown in Fig. 2.

2.2 DEM-FEM coupling simulation approach

In order to simulate the real process of shot peening as more as possible, the integrated DEM-FEM coupling simulation approach was developed in this work. Different from the
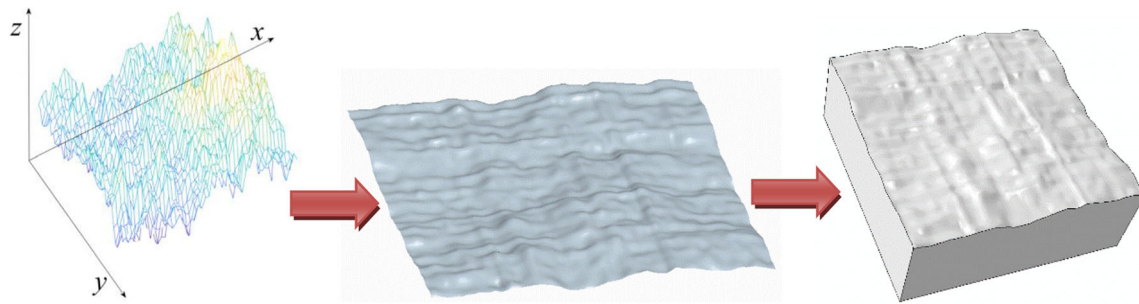
Fig. 1 Rough surfaces created by MATLAB and Pro/E

conventional FEM-DEM coupling simulation strategy, which performed the numerical simulations of shot peening process by linking DEM software (such as EDEM, PFC3D) with FEM software (such as ABAQUS/Explicit, ANSYS/Ls-Dyna), the present work implemented the DEM code into the generated FEM input file of ABAQUS code; in other words, the only ABAQUS code was used in this work. When compared with the conventional FEM-DEM coupling simulation strategy, it is extremely convenient and efficient for the integrated FEM-DEM coupling simulation of multiple shot impacts on the original rough surface. The simulation scheme used in this work is shown in the following Fig. 3.

As seen in Fig. 3, the discrete element method (DEM) was used to simulate the movement behaviors of shot flow, and both the shot-shot interaction and shot-target interaction are taken into consideration. In the discrete element model of shot flow, the shot was modeled as a particle and meshed by single-node element of PD3D in ABAQUS code. The particle was regarded as a rigid sphere with the same diameter as the real shot diameter, and the material property parameters of the real shot were also used to characterize the material property of the particle, such as the mass density of 7800 kg/m^3, elastic modulus of 210 GPa, and Poisson's ratio of 0.3. The particles were dynamically generated through the nozzle outlet by Particle Generator supplied by ABAQUS code, and were sprayed onto the target surface to be peening. The nozzle with a circular cross section was modeled as a disk-shape plane and was meshed by single finite element of S4R in ABAQUS code.

In order to simplify the calculation process and reduce the computation cost, the diameter of the nozzle is 3 mm and the distance between the nozzle and the target surface is 15 mm. The mass flow rate of particles per unit area of nozzle outlet (M_s) is related to flow speed (Q) and volume fraction (a) of particles and is expressed as

$$M_s = \rho a Q \tag{6}$$

where the flow speed of particles was assumed to be a constant of 50 m/s, the volume fraction is 0.8, and ρ is the mass density of particles.

The general contact was adopted to compute the interactions of particle-particle (shot-shot) and particle-target (shot-target). The element-based surfaces of both particles and target were defined at first, and the contact relations of particle surface-particle surface and particle surface-target surface were then specified, respectively. The friction coefficient between particle surface and particle surface was assigned to be 0.3. For the particle-particle (shot-shot) interaction, the Hertz contact model was used, which establishes the relation between the contact force (F_n) and the penetration displacement of any two contacting spherical particles.

$$F_n = \frac{4}{3} E^* \sqrt{R^*} \delta^{\frac{3}{2}} \tag{7}$$

$$E^* = \left(\frac{1-v_1^2}{E_1} + \frac{1-v_2^2}{E_2} \right)^{-1} \tag{8}$$
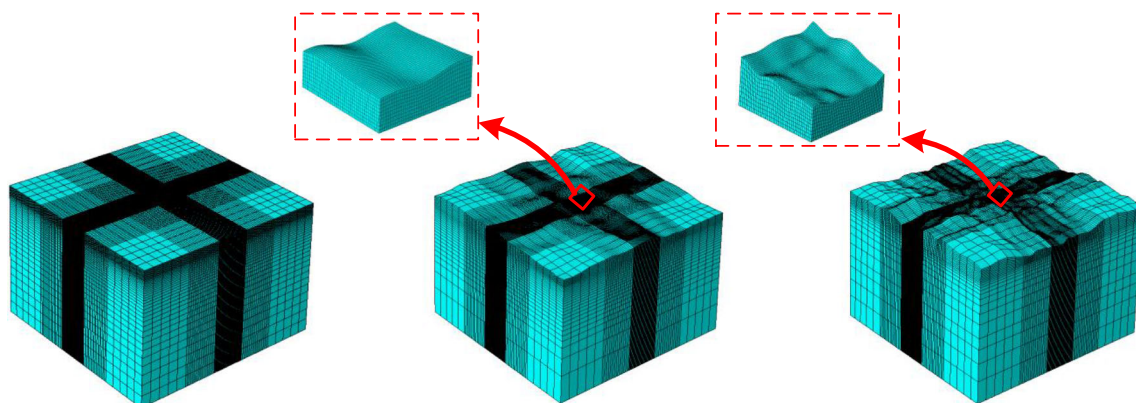
Fig. 2 Target models with the original rough surfaces: **a** $R_{a0} = 0$ μm, **b** $R_{a0} = 26.7$ μm, and **c** $R_{a0} = 50.1$ μm
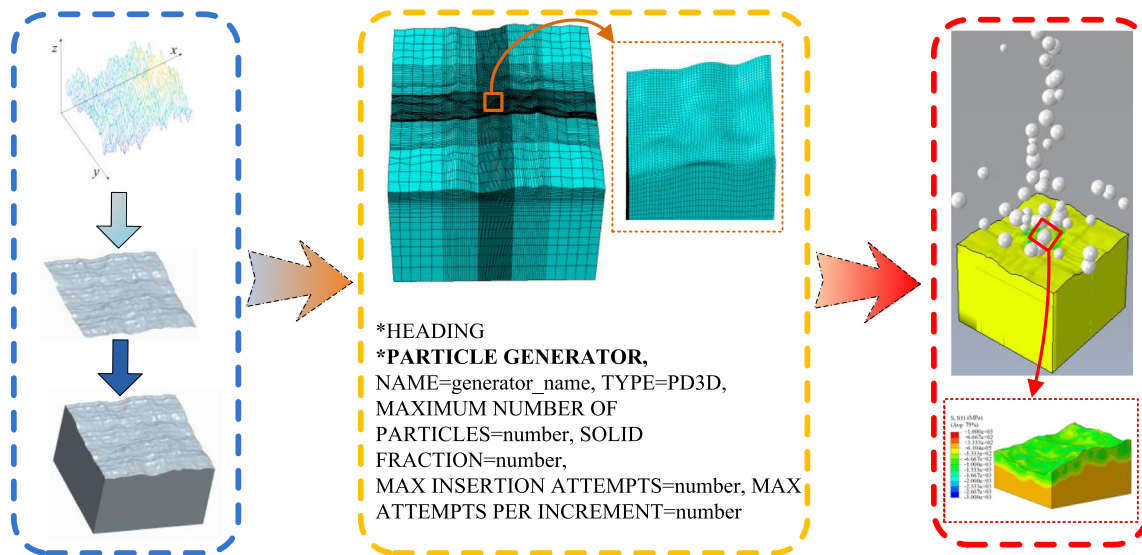
Fig. 3 DEM-FEM coupling simulation of shot peening process

$$R^* = \frac{R_1 R_2}{R_1 + R_2} \tag{9}$$

where E_1 (or E_2), v_1 (or v_2), and R_1 (or R_2) are the elastic modulus, Poisson's ratios, and radius of any two shots, respectively. To simulate the real process of shot peening, the rigid contact without penetration between any two particles was taken into consideration in this work.

For the simulation of the contact between the particle (shot) surface and target surface, the penalty function method with the friction coefficient of 0.3 was used. The target to be peening was modeled as a three-dimensional finite element model with the length of 6 mm, width of 6 mm, and height of 4 mm, as shown in Fig. 2. The target model was meshed by the finite elements with the type of C3D8R in ABAQUS code, and the size of the finest element is 20 μm [58, 59]. The bottom surface of the target model was fixed, and the top surface with the given original surface roughness was impacted by a large number of particles (shots). Considering that the target model is a deformable body, and the residual stresses and surface roughness induced by shot peening are the results of the elastic-plastic deformation associated with the high strain rate (~10^5 s^{-1}), the Johnson-Cook (JC) model was employed as the material constitutive model to characterize the dynamic stress-strain responses resulting from the multiple shot impacts.

$$\sigma_f = \left[A + B\overline{\varepsilon}_p^n\right] \cdot \left[1 + C\ln\left(\frac{\dot{\overline{\varepsilon}}_p}{\dot{\overline{\varepsilon}}_0}\right)\right] \cdot \left[1 - \left(\frac{T-T_r}{T_m-T_r}\right)^m\right] \tag{10}$$

where A is the initial yield strength of the material at room temperature of T_r; B is the strain hardening coefficient; C represents the strain rate sensitivity; $\overline{\varepsilon}_p$, $\dot{\overline{\varepsilon}}_p$, and $\dot{\overline{\varepsilon}}_0$ represent the equivalent plastic strain, equivalent plastic strain rate, and

reference plastic strain rate, respectively; T represents the temperature; T_m is the melting temperature; n and m are related to the strain hardening and thermal softening effects, respectively. The JC model parameters of TC4 titanium alloy are listed in Table 1 [60].

2.3 Validation of DEM-FEM coupling simulation

The shot peening experiments taken from literatures [61, 62] were adopted to validate the integrated DEM-FEM coupling simulation of shot peening process. The shot peening experiments [61, 62] were conducted with the shot peening coverage of 100% and Almen intensity of 0.3 mmA. The nozzle was perpendicular to the target surface, which indicates that a large number of shots vertically impacted on the target surface, and the original surface roughness was not taken into consideration. The used shot type was S230 which is corresponding to the average diameter of 0.6 mm. According to the following formula [63], the shot impact velocity was estimated as 50 m/s.

$$v = \frac{16.35 \times P}{1.53 \times M + P} + \frac{29..50 \times P}{0.598 \times D + P} + 4.83 \times P \tag{11}$$

where P (bar) is the supplied air pressure, M (kg/min) is the mass flow rate of the shots (or particles), D (mm) is the averaged shot diameter, and v (m/s) is the shot impact velocity.

The shot peening experiments [61, 62] were simulated by using the integrated DEM-FEM coupling simulation approach. In order to take into account the effect of shot diameter, two kinds of the integrated DEM-FEM coupling simulations were carried out in this work and were named as Case 1 and Case 2, respectively. Case 1 used the same shot diameter of 0.6 mm, and Case 2 used the uniformly distributed shot diameters in the range from 0.4 to 0.8 mm, wherein the

Table 1 JC parameters of TC4 titanium alloy [60]

A (MPa)	B (MPa)	C	n	m	T_r (K)	T_m (K)	$\bar{\bar{\varepsilon}}_0$ (s−1)
1098	1092	0.014	0.93	1.1	298	1878	1.0

average value is 0.6 mm. According to the Avrami formula, i.e., Eq(12), which is generally used to evaluate the shot peening coverage, 400 shots (or particles) were needed to be generated to simulate the shot peening process with 100% coverage through the trial calculations, and then 200% coverage needed 800 shot impacts.

$$C_{SP} = 100\% \times \left[1 - \exp\left(-N_{SP}\frac{\pi \cdot r^2}{S_n}\right)\right] \quad (12)$$

where C_{SP} represents the shot peening coverage, N_{SP} is the number of shots (or particles), S_n is the area size of the region to be peening which was thought to be the area size of the nozzle considering that the multiple shots were driven to impact on the target surface vertically from the stationary nozzle, and r is the radius of the dimple produced by single shot vertical impact and $r = 0.11$ mm resulting from the finite element computation.

In order to reduce the edge effects of shot-peened region as more as possible, the central region with the dimension of $1mm \times 1mm \times 0.3mm$ was regarded as the reference for analyzing the numerical simulation results. The predicted distributions of the residual stresses induced by shot peening are shown in Fig. 4, wherein the only quarter of the shot-peened target model is presented and the symbol of "S11" denotes the in-plane stress along the x-axis direction, σ_x. It should be noted that the average values of residual stresses in the x and y direction are assumed to be equal, $\sigma_x = \sigma_y$, since the shot peening process is considered to be homogeneous when the shot peening coverage is larger than 100%. As seen from Fig.
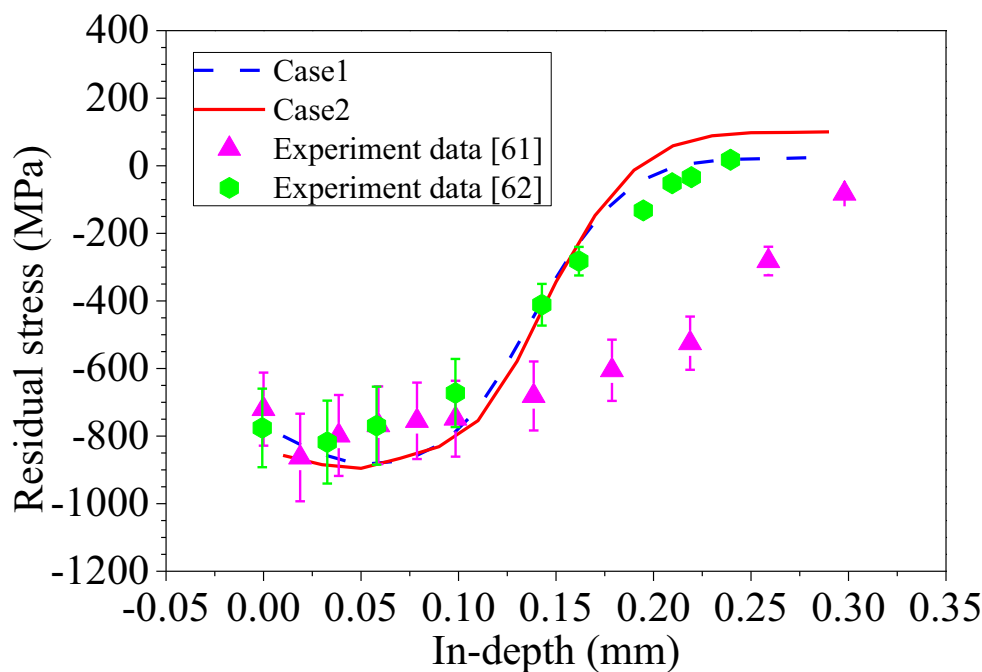
4, the compressive residual stresses are produced in the shot-peened surface and subsurface layers, and the maximum compressive residual stresses are located in the subsurface. For keeping the stress equilibrium of the whole shot-peened target model, the tensile residual stresses are resultantly produced below the compressive residual stresses. It is noted that there are some tensile residual stresses in the shot-peened surface due to the non-uniform elastic-plastic deformations under 100% shot peening coverage. By comparing the two simulation results of Case 1 and Case 2, there is little difference between them; it therefore reveals that the shot-peened residual stresses are insignificant sensitive to the changes of shot diameters when the average value remains a constant.

To compare the numerically predicted results of the integrated DEM-FEM coupling simulation with the experimentally measured results, the standard normal distribution function was employed to process the statistical data of the resultant residual stresses outputting from each element layer along the thickness direction within the reference region, and the calculated mathematic expectation was used to represent the in-depth residual stresses, as shown in Fig. 5. With the different shot diameters, the insignificant difference of the in-depth residual stresses can be observed by comparing Case 1 with Case 2. Additionally, whether Case 1 or Case 2, the predicted in-depth residual stresses are in good agreement with the experimental results. It is therefore demonstrated that the integrated DEM-FEM coupling simulation approach only based on ABAQUS code has the capability of simulating the real shot peening process very accurately.

Fig. 4 Predictions of the residual stresses induced by shot peening. **a** Case 1. **b** Case 2

S, S11 (MPa)
(Avg: 75%)

+1.000e+03
+6.667e+02
+3.333e+02
+6.104e-05
−3.333e+02
−6.667e+02
−1.000e+03
−1.333e+03
−1.667e+03
−2.000e+03
−2.333e+03
−2.667e+03
−3.000e+03

Case 1

Case 2

(a)   (b)
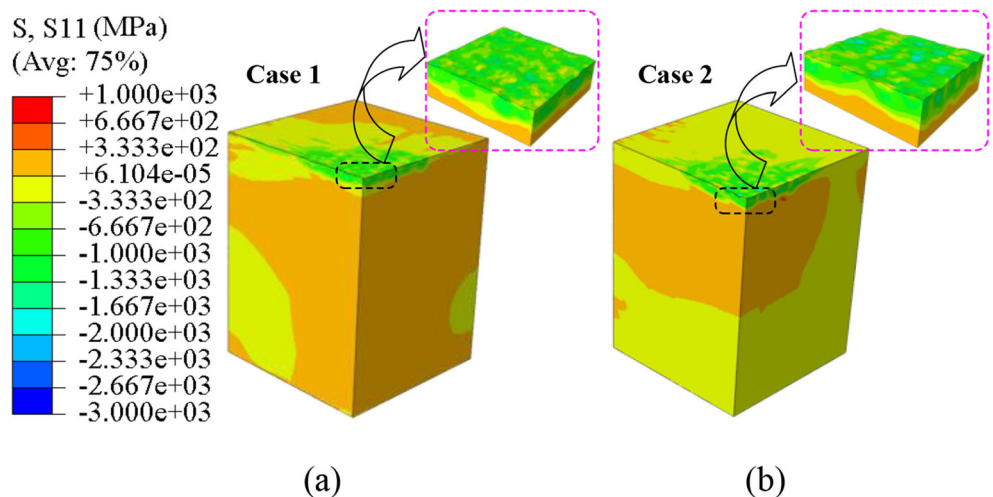
Fig. 5 Comparison between the predicted residual stresses and experimental results

3 Results and discussion

3.1 Effect of the original surface roughness
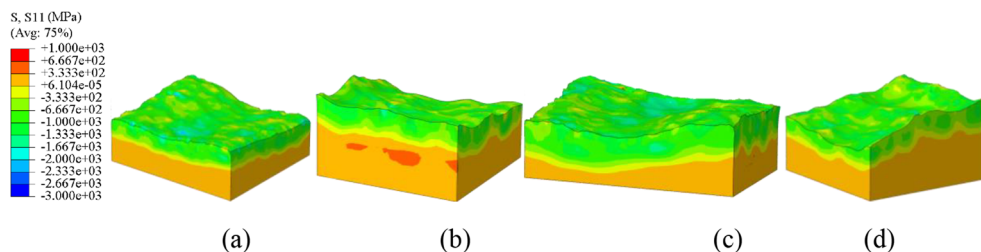
3.1.1 Residual stresses

Under the shot peening coverage of 100% and impact angle of 90, for the three kinds of target models associated with the different original surface roughness (R_{a0} = 0 μm), (26.7 μm), and 50.1 μm), the shot peening-induced residual stresses are shown in Fig. 6. The much similar distributions of the resultant residual stresses as Fig. 4 can be observed in Fig. 6, wherein the beneficial compressive residual stresses were introduced into the shot-peened surface and subsurface layers of target models. As seen from Fig. 6, with the same original surface roughness, by comparing Fig. 6a with Fig. 6c (or comparing Fig. 6b with Fig. 6d), it is hardly to distinguish the difference in the distributions of the shot-peened residual stresses in the Case 1 and Case 2, which is consistent with the phenomenon as shown in Fig. 4.

Figure 7 shows the statistical results of the surface residual stresses from Fig. 6, wherein the x-coordinates denote the

residual stresses and y-coordinates denote the percentages of the number of the elements associated with the residual stresses within the reference area. The standard normal distribution function was employed to process the statistical data of the surface residual stresses, and the standard deviation was calculated accordingly, as shown in Fig. 7. The standard deviations corresponding to the distributions of the residual stresses in Fig. 6 were 430.2 MPa, 344.9 MPa, 462.3 MPa, and 335.8 MPa, respectively. It is of interest to notice that the uniformity of the surface residual stresses in the case of R_{a0} = 50.1 μm is better than that in the case of R_{a0} = 26.7 μm for the same shot diameter, whereas the uniformities of the surface residual stresses in the Case 1 and Case 2 are not obviously different for the same original surface roughness. It therefore reveals that the surface residual stresses are more sensitive to the original surface roughness than the changes of shot diameters with the average value remaining a constant.

Applying the standard normal distribution function to process the predicted residual stresses outputting from each element layer in the thickness direction, the mathematic expectations of the statistical data are shown in Fig. 8, which represent the in-depth residual stresses. Different from the case of

Fig. 6 Distribution of the residual stresses induced by shot peening: **a** R_{a0} = 26.7 μm & Case1, **b** R_{a0} = 50.1 μm & Case1, **c** R_{a0} = 26.7 μm & Case 2, and **d** R_{a0} = 50.1 μm & Case 2
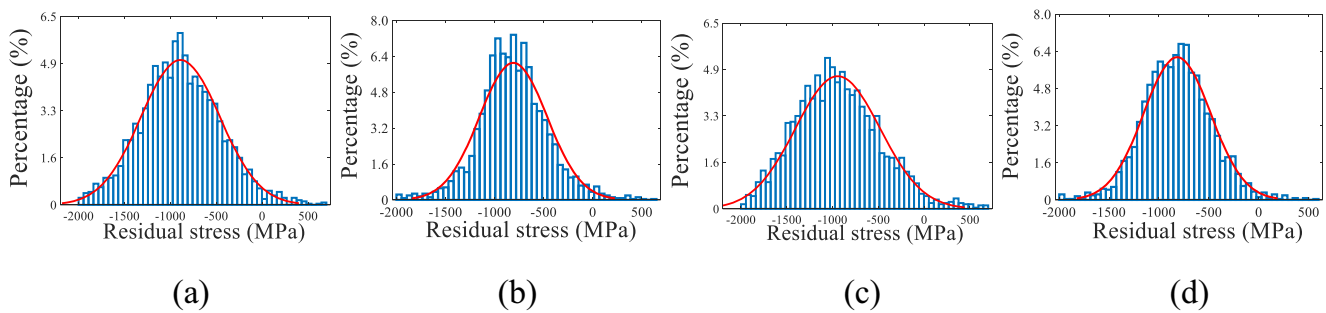
Fig. 7 Statistical analysis of the residual stresses induced by shot peening: **a** $R_{a0} = 26.7$ μm & Case1, **b** $R_{a0} = 50.1$ μm & Case1, **c** $R_{a0} = 26.7$ μm & Case 2, and **d** $R_{a0} = 50.1$ μm & Case 2

$R_{a0} = 0$ μm (the target model without the original surface roughness), for the target models associated with the original surface roughness of $R_{a0} = 26.7$ μm or 50.1 μm, the maximum compressive residual stresses are located in the shot-peened surface, and the compressive residual stresses within the surface and subsurface layers are relatively larger in the case of $R_{a0} = 50.1$ μm than that in the case of $R_{a0} = 26.7$ μm, whereas the increasing tensile residual stresses are produced with the increase in the original surface roughness. By comparing Fig. 8a with Fig. 8b, it can be concluded that there is a slight difference in the distributions of the shot-peened residual stresses when the original surface roughness remains a constant ($R_{a0} = 0$ μm or 26.7 μm or 50.1 μm). It therefore indicates that the residual stresses induced by shot peening are insignificantly sensitive to the changes of shot diameters when the average value remains a constant once again.

3.1.2 Surface roughness

The shot-peened surface topographies in the different shot peening conditions are shown in Fig. 9. Under the multiple shot impacts, many indentations and ridges were produced in the shot-peened surface, as seen from Fig. 9, wherein the symbol "U3" denotes the normal displacement which can

indicate the non-uniform elastic-plastic deformations indirectly. For the same shot peening condition (Case 1 or Case 2), with the increase of the original surface roughness, the more obvious ridges produced in the local valley regions of the original rough surface can be observed carefully, which could be explained by the reason that the local peak regions were prior to be impinged by multiple shots. On the other hand, when the original surface roughness remains a constant, the more obvious indentations and ridges can be observed in the Case 2; it reveals that the changes of shot diameters would result in the more non-uniform plastic deformations in the shot-peened surface.

According to Eq. (4) and Eq. (5), the values of R_a and R_q with respect to the shot-peened and un-peened surfaces are shown in Fig. 10. For the target model without the original surface roughness, i.e., $R_{a0} = 0$ μm or $R_{q0} = 0$ μm, the shot-peened surface roughness of $R_a = 3.5$ μm and 4.2 μm (or $R_a = 4.3$ μm and 5.3 μm) were produced in the Case 1 and Case 2, respectively. It indicates that the variable shot diameters would produce the larger surface roughness in the case of $R_{ao} = 0$ μm, although the average value of the variable shot diameters is the same as the constant shot diameter. However, as seen in Fig. 10, when compared with the initial surface roughness, for the target models associated with the original
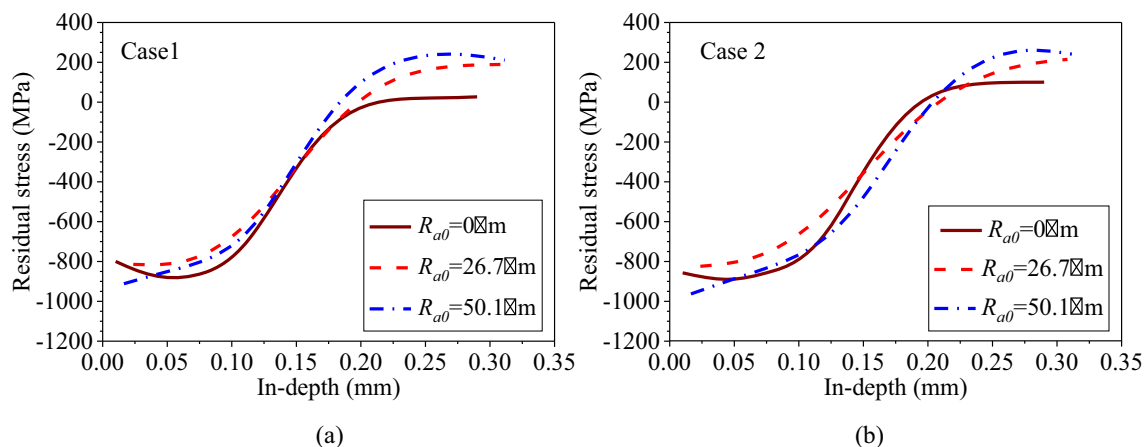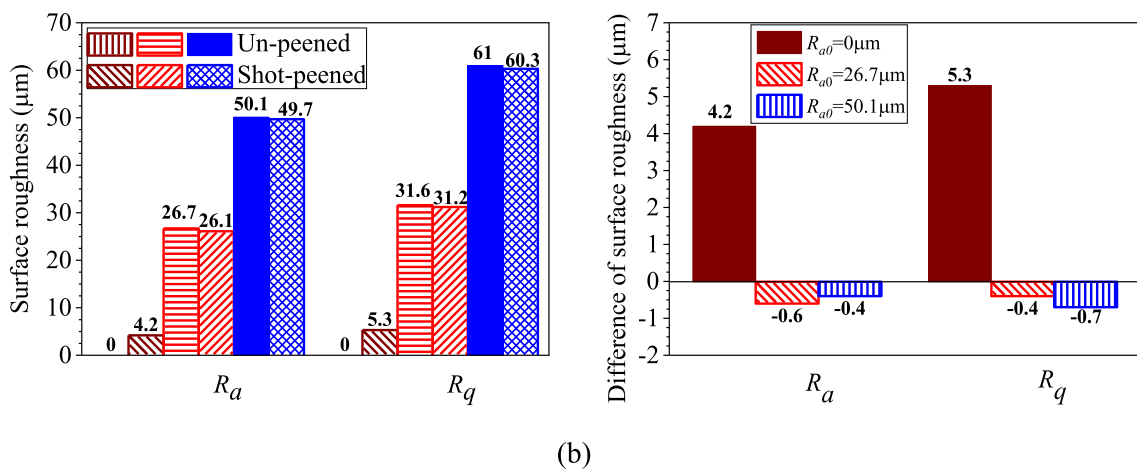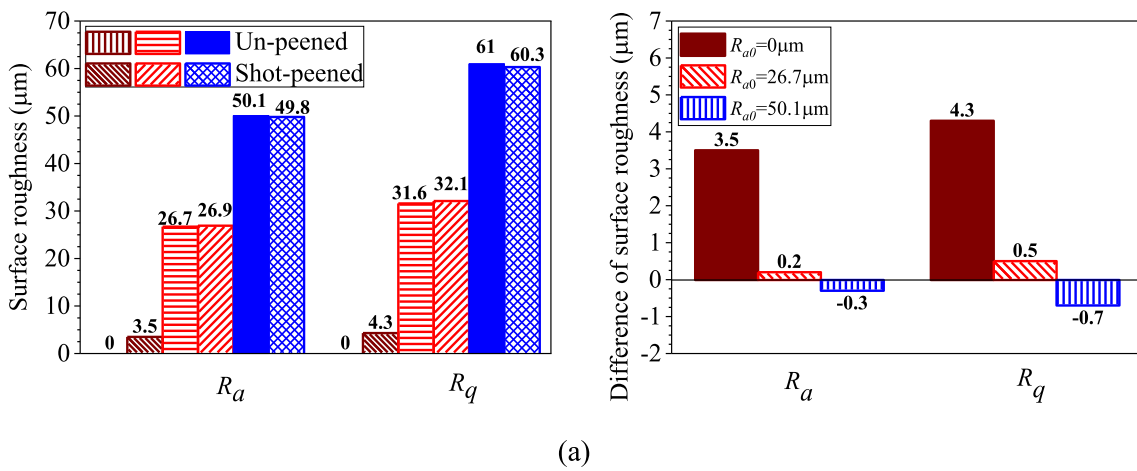

Fig. 8 In-depth residual stresses resulting from the target models with different original surface roughness. **a** Case 1. **b** Case 2
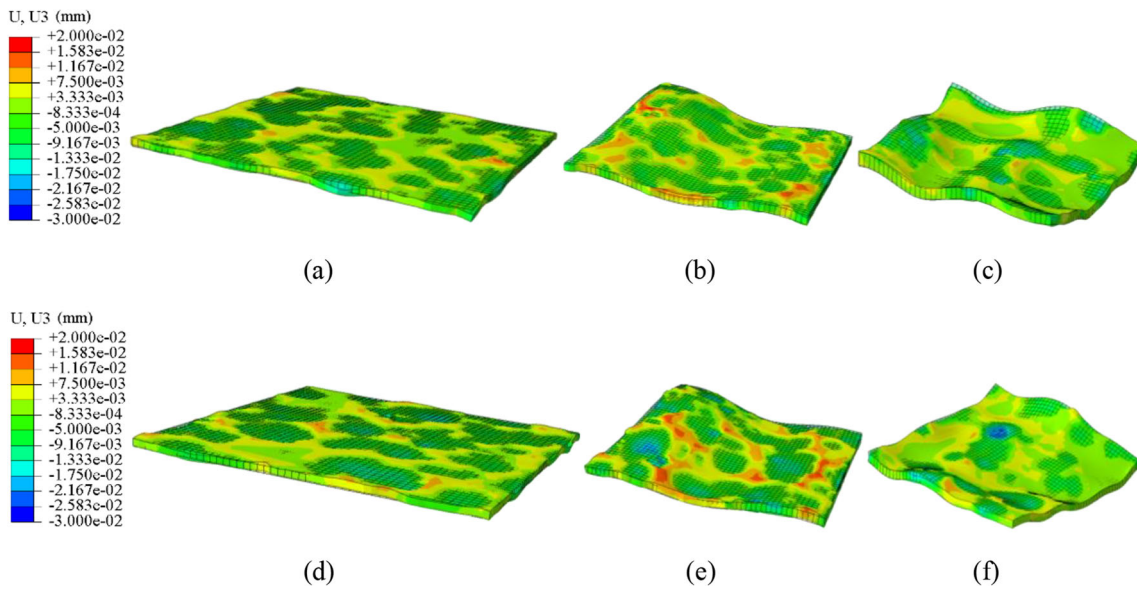
Fig. 9 Surface topographies produced by shot peening: **a** R_{a0} = 0 μm & Case 1, **b** R_{a0} = 26.70 μm & Case 1, **c** R_{a0} = 50.1 μm & Case 1, **d** R_{a0} = 0 μm & Case 2, **e** R_{a0} = 26.7 μm & Case 2, and **f** R_{a0} = 50.1 μm & Case 2

Fig. 10 Un-peened and shot-peened surface roughness and their differences. **a** Case 1. **b** Case 2

surface roughness of $R_{ao} = 26.7$ μm or $R_{q0} = 31.6$ μm, the slight increase of the surface roughness is produced by shot peening in the Case 1, and the shot-peened surface roughness decreases unexpectedly for the target model associated with the original surface roughness of $R_{a0} = 50.1$ μm (or $R_{q0} = 61$ μm), and the similar phenomenon can be found in the Case 2 for $R_{a0} = 26.7$ μm. It is therefore concluded that shot peening could be conductive to reducing the larger original surface roughness of TC4 titanium alloy, and the variable shot diameters would be more effective in this respect.

3.2 Effect of shot impact angle

3.2.1 Residual stresses

Three kinds of shot impact angles, $a = 60°$, $75°$, and $90°$, were set to investigate the effect of shot impact angle on the shot-peened residual stresses and surface roughness, and the two kinds of target models associated with the original surface roughness of $R_{a0} = 0$ μm and 50.1 μm were used to be peening under the 100% coverage. The residual stress fields induced by shot peening are shown in Fig. 11. Herein, the standard normal distribution function was also used to process the statistical data of the surface residual stresses, and standard deviations corresponding to the Fig. 11 a, b, c, and d were calculated as 349.9 MPa, 339.6 MPa, 308.9 MPa, and 310.3 MPa, respectively. It reveals that the insignificant difference can be observed in the distribution uniformity of the shot-peened surface residual stresses with respect to the shot impact angles of 60° and 75°; however, the relatively more uniform surface compressive residual stresses could be obtained in the target model with the original surface roughness of $R_{a0} = 50.1$ μm, when compared with that in the case of $R_{a0} = 0$ μm.

With the mathematic expectation of the standard normal distribution function, the in-depth residual stresses with respect to the shot impact angles of 60°, 75°, and 90° are shown in Fig. 12. From the figures, it is clearly obvious that the larger compressive residual stresses within the shot-peened surface and subsurface layers are produced in the case of $a = 90°$, when compared with the cases of $a = 60°$ and 75°. The depth

of the compressive residual stresses increases with the increase of shot impact angle in the target model without the original surface roughness (i.e., $R_{a0} = 0$ μm). However, for the target model associated with the original surface roughness of $a = 50.1$ μm, there is insignificant difference in the shot-peened compressive residual stresses with respect to the shot impact angles of 60° and 70°

3.2.2 Surface roughness

The shot-peened surface roughness with respect to the shot impact angles of 60°, 75°, and 90° are shown in Fig. 13. As seen from Fig. 13a, for the target model without the original surface roughness, with the increase of the shot impact angles, the values of R_a and R_q increase, which indicates that the shot-peened surface roughness increases accordingly. However, for the target model associated with the original surface roughness of $R_{a0} = 50.1$ μm, it should be noted that the shot-peened surface roughness is smaller than the original surface roughness, as seen in Fig. 13b and c, which reveals that the shot peening would be conductive to reducing the larger original surface roughness. On the other hand, for the target model associated with the larger original surface roughness of $R_{a0} = 50.1$ μm, the insignificant difference in the reduction of the shot-peened surface roughness in Fig. 13c reveals that the shot-peened surface roughness is almost insensitive to the shot impact angles in the range from 60° to 90°.

3.3 Effect of shot peening coverage

3.3.1 Residual stresses

In order to investigate the effect of shot peening coverage on the resultant residual stresses and surface roughness, the comparative simulations of shot peening processes with 100% and 200% coverages were carried out. Under the shot peening coverage of 200%, for the two kinds of target models associated with the original surface roughness of $R_{a0} = 0$ μm and 50.1 μm, the simulation results of the shot-peened residual stresses are shown in Fig. 14a and b. The standard deviations
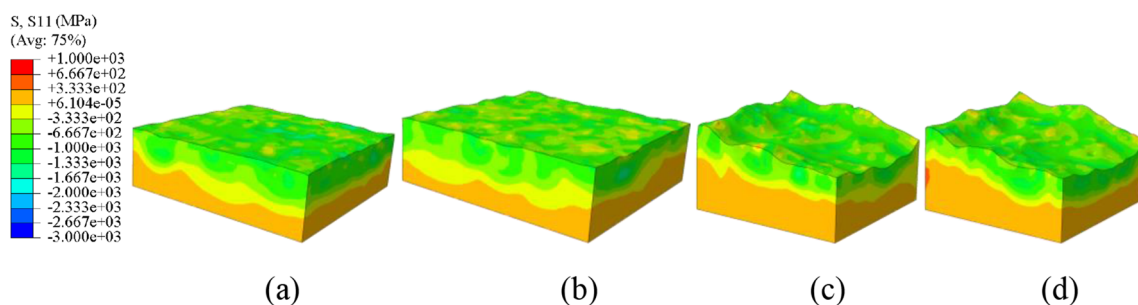
Fig. 11 Distributions of the residual stresses induced by shot peening with respect to different shot impact angles: **a** $a = 60°$ & $R_{a0} = 0$ μm, **b** $a = 75°$ & $R_{a0} = 0$ μm, **c** $a = 60°$ & $R_{a0} = 50.1$ μm, and **d** $a = 75°$ & $R_{a0} = 50.1$ μm
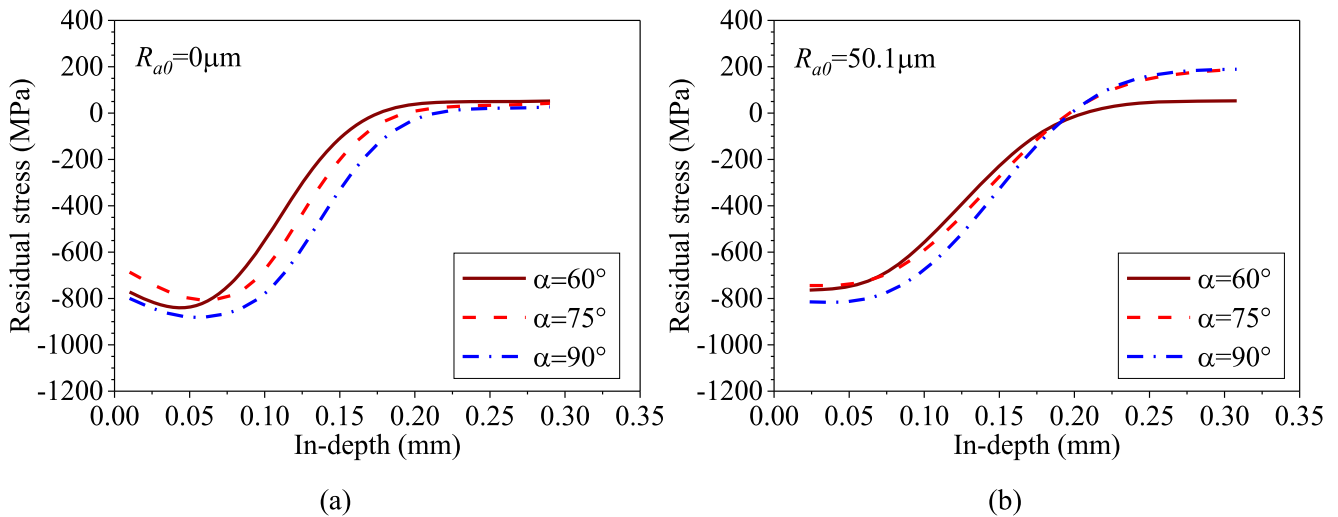
Fig. 12 In-depth residual stresses induced by shot peening with respect to the different shot impact angles. **a** $R_{a0} = 0$ μm. **b** $R_{a0} = 50.1$ μm

of the surface residual stresses were calculated as 448.8 MPa and 345.4 MPa, respectively. It indicates that the larger original surface roughness could make the shot-peened surface residual stresses to be more uniform. With the mathematic expectation of the standard normal distribution function, the in-depth residual stresses corresponding to Fig. 14 a and b are shown in Fig. 14c. It is obvious that the larger compressive residual stresses are produced in the shot-peened surface and subsurface layers under 200% coverage than that in the case of 100% coverage. As seen in Fig. 14c, under the same shot peening coverage of 100% or 200%, when compared with the in-depth residual stresses resulting from the target model without the original surface roughness, the smaller compressive residual stresses while the larger tensile residual stresses were produced in the target model with the original surface roughness of $R_{a0} = 50.1$ μm. It therefore reveals that the larger original surface roughness of $R_{a0} = 50.1$ μm is

unfavorable to the introduction of the beneficial compressive residual stresses induced by shot peening.

3.3.2 Surface roughness

For the two kinds of target models associated with the original surface roughness of $R_{a0} = 0$ μm and 50.1 μm, the simulated surface roughness under the 100% and 200% coverages are shown in Fig. 15. It is of interest to notice that the opposite trends of the shot-peened surface roughness can be observed in the cases of $R_{a0} = 0$ μm and 50 μm. With the increasing shot peening coverage from 100 to 200%, the shot-peened surface roughness increases to 4.5 μm from 3.5 μm in the case of $R_{a0} = 0$ μm, whereas the shot-peened surface roughness decreases to 49.6 μm from 49.8 μm in the case of $R_{a0} = 50.1$ μm. It indicates that the increase of shot peening

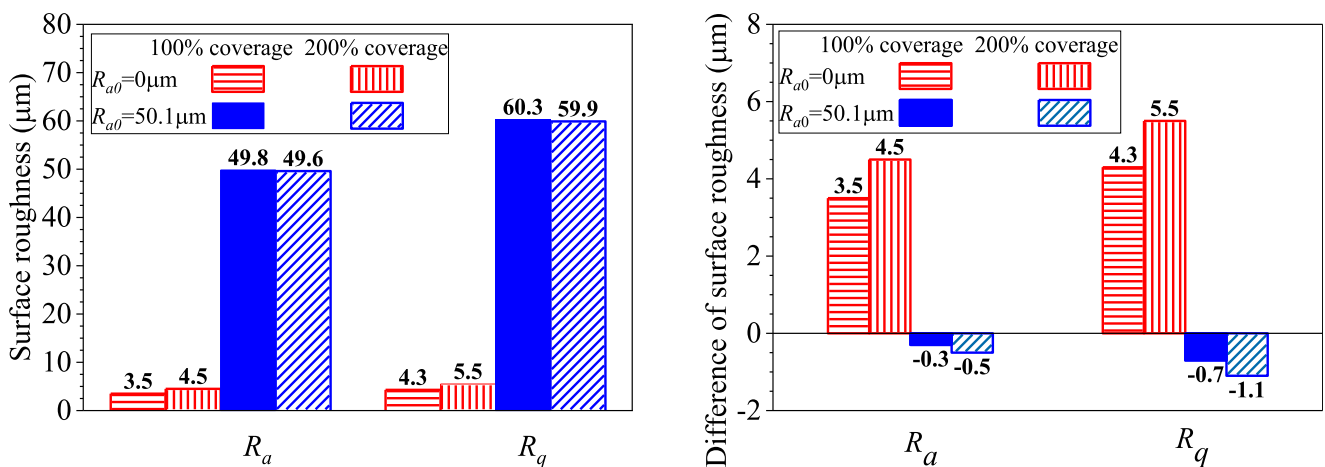**Fig. 13** Shot-peened surface roughness under different shot impact angles and their difference. **a** $R_{a0} = 0$ μm. **b** $R_{a0} = 50.1$ μm
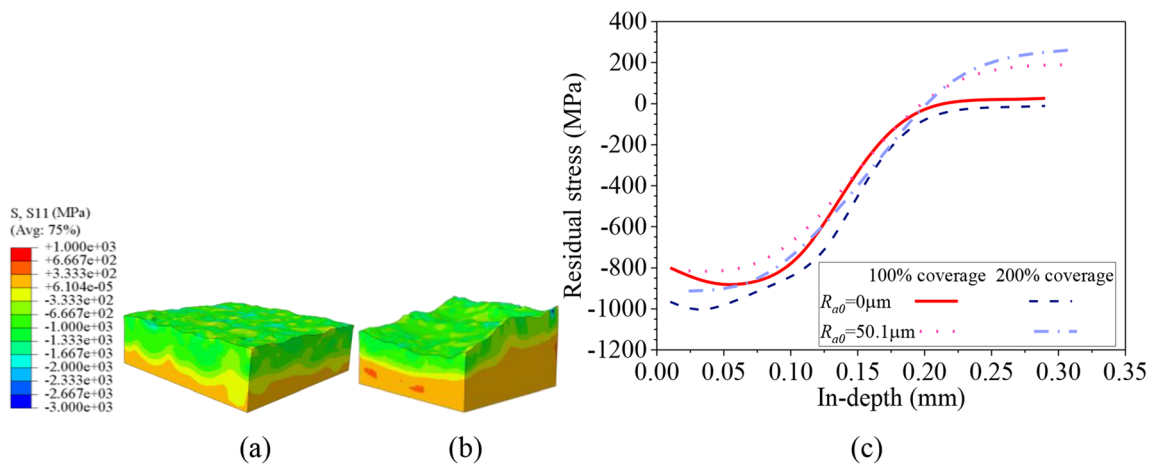
Fig. 14 Residual stresses induced by shot peening under 200% coverage: **a** $R_{a0} = 50.1$ μm , **b**, and **c** in-depth residual stresses

coverage could be conductive to reducing the larger original surface roughness.

4 Conclusions

Based on the analysis platform of ABAQUS code, the integrated DEM-FEM coupling simulation approach was developed to simulate the real process of shot peening, and the numerically predicted in-depth residual stresses are in good agreement with the experimentally measured results, which verifies the validity of this approach. In order to investigate the effect of the original rough surface on the shot-peened residual stresses and surface roughness, two kinds of target models associated with the original surface roughness of $R_{a0} = 26.7$ μm and 50.1 μm were respectively created by taking advantage of the Gaussian distribution incorporated with the exponential autocorrelation function, and the target model without the original surface roughness was utilized for

reference purposes. By using the integrated DEM-FEM coupling simulation approach, the effects of the shot impact angle and shot peening coverage on the shot-peened residual stresses and surface roughness were further analyzed and discussed in detail. The obtained conclusions were drawn as follows.

1. The residual stresses induced by shot peening are insignificant sensitive to the changes of shot diameters when the average value remains a constant.
2. Under the same shot peening condition, for the target model associated with the original surface roughness of $R_{a0} = 50.1$ μm, the larger compressive residual stresses are produced, and the shot-peened surface roughness is smaller than the original surface roughness, when compared with the target model associated with the original surface roughness of $R_{a0} = 26.7$ μm.
3. The larger compressive residual stresses induced by shot peening are corresponding to the shot impact angle of 90°, and the shot-peened residual stresses and surface
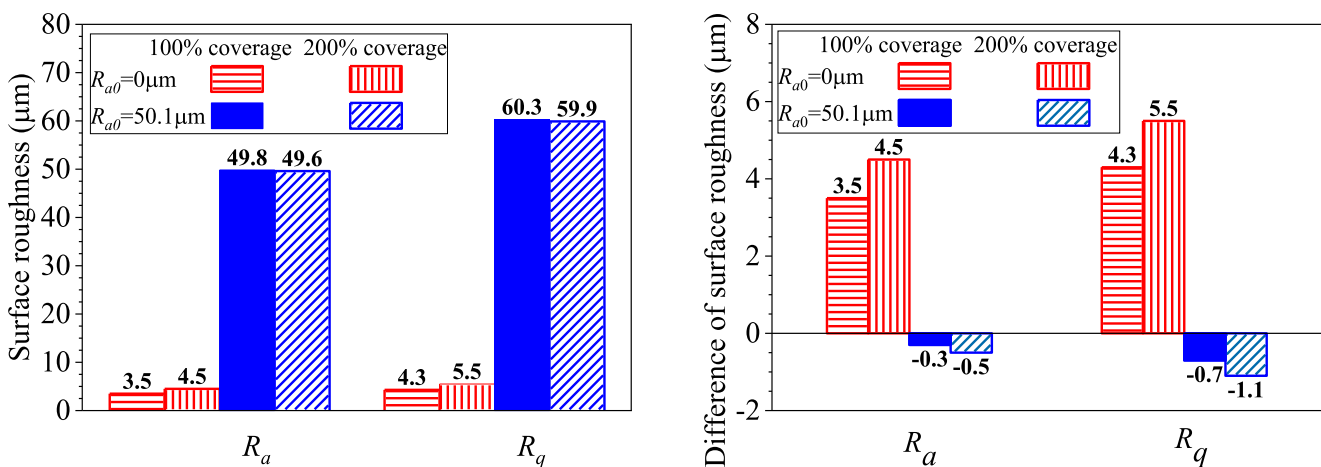

Fig. 15 Shot-peened surface roughness under 100% and 200% coverage and their difference

roughness with respect to the shot impact angles of 60° and 75° are insignificant different in the target model associated with the original surface roughness of R_{a0} = 50.1 μm.

4. With the shot peening coverage increasing to 200% from 100%, the compressive residual stresses in the shot-peened surface and subsurface layers increases, the shot-peened surface roughness increases in the case of R_{a0} = 0 μm while decreases in the case of R_{a0} = 50.1 μm when compared with the original surface roughness.

Declarations

Ethics approval It is approved that the paper is original and has been written based on the authors' own finding. All the figures and tables are original, and every expression from other published works were acknowledged and referenced.

Consent to participate All authors are aware and satisfied of the authorship order and correspondence of the paper.

Consent for publication All authors are satisfied that the last revised version of the paper is published without any change.

Competing interests The authors declare no competing interests.

References

1. Tan L, Yao C, Zhang D, Ren J, Shen X, Zhou Z (2020) Effects of different mechanical surface treatments on surface integrity of TC17 alloys. Surf Coat Technol 398:126073. https://doi.org/10.1016/j.surfcoat.2020.126073

2. Bagherifard S (2019) Enhancing the structural performance of lightweight metals by shot peening. Adv Eng Mater 21(7):1801140. https://doi.org/10.1002/adem.201801140

3. Karimbaev R, Pyun YS, Maleki E, Unal O, Amanov A (2020) An improvement in fatigue behavior of AISI 4340 steel by shot peening and ultrasonic nanocrystal surface modification. Mat Sci Eng A-Struct 791:139752. https://doi.org/10.1016/j.msea.2020.139752

4. Omari MA, Mousa HM, Al-Oqla FM, Aljarrah M (2019) Enhancing the surface hardness and roughness of engine blades using the shot peening process. Int J Miner Metall Mater 26(8):999–1004. https://doi.org/10.1007/s12613-019-1818-5

5. Wang C, Wu G, He T, Zhou YJ, Zhou ZC (2020) Numerical study of fatigue crack propagation in a residual stress field induced by shot peening. J Mater Eng Perform 29(8):5525–5539. https://doi.org/10.1007/s11665-020-05029-9

6. Wang C, Lai YB, Wang L, Wang CL (2020) Dislocation-based study on the influences of shot peening on fatigue resistance. Surf Coat Technol 383:125247. https://doi.org/10.1016/j.surfcoat.2019.125247

7. Bag A, Lévesque M, Brochu M (2020) Effect of shot peening on short crack propagation in 300M steel. Int J Fatigue 131:105346. https://doi.org/10.1016/j.ijfatigue.2019.105346

8. Chadwick DJ, Ghanbari S, Bahr DF, Sangid MD (2018) Crack incubation in shot peened AA7050 and mechanism for fatigue enhancement. Fatigue Fract Eng Mater Struct 41(1):71–83. https://doi.org/10.1111/ffe.12652

9. Liu YG, Li MQ, Liu HJ (2017) Nanostructure and surface roughness in the processed surface layer of Ti-6Al-4V via shot peening. Mater Charact 123:83–90. https://doi.org/10.1016/j.matchar.2016.11.020

10. Zhang C, Rong H, Song G, Hu K (2019) Effect of surface roughness by shot peening on stress corrosion cracking behavior of pure titanium welded joints in HCl solution. Acta Metall Sin 55(10):1282–1290. https://doi.org/10.11900/0412.1961.2019.00056

11. Wen Y, Liu P, Xie LC, Wang Z, Wang LQ, Lu WJ, Jiang CH, Ji V (2020) Evaluation of mechanical behavior and surface morphology of shot-peened Ti-6Al-4V alloy. J Mater Eng Perform 29(1):182–190. https://doi.org/10.1007/s11665-020-04565-8

12. Ghanbari S, Bahr DF (2020) Predictions of decreased surface roughness after shot peening using controlled media dimensions. J Mater Sci Technol 58:120–129. https://doi.org/10.1016/j.jmst.2020.03.075

13. Yang C, Li MQ (2020) 3D surface morphology and performance of TC17 processed by surface severe plastic deformation. Surf Coat Technol 397:125995. https://doi.org/10.1016/j.surfcoat.2020.125995

14. Liu YG, Li HM, Li MQ (2020) Roles for shot dimension, air pressure and duration in the fabrication of nanocrystalline surface layer in TC17 alloy via high energy shot peening. J Manuf Process 56:562–570. https://doi.org/10.1016/j.jmapro.2020.05.019

15. Lin Q, Liu H, Zhu C, Chen D, Zhou S (2020) Effects of different shot peening parameters on residual stress, surface roughness and cell size. Surf Coat Technol 398:126054. https://doi.org/10.1016/j.surfcoat.2020.126054

16. Ongtrakulkij G, Khantachawana A, Kondoh K (2020) Effects of media parameters on enhance ability of hardness and residual stress of Ti6Al4V by fine shot peening. Surf Interfaces 18:100424. https://doi.org/10.1016/j.surfin.2019.100424

17. Wu J, Liu H, Wei P, Lin Q, Zhou S (2020) Effect of shot peening coverage on residual stress and surface roughness of 18CrNiMo7-6 steel. Int J Mech Sci 183:105785. https://doi.org/10.1016/j.ijmecsci.2020.105785

18. Maleki E, Unal O (2018) Roles of surface coverage increase and re-peening on properties of AISI 1045 carbon steel in conventional and severe shot peening processes. Surf Interfaces 11:82–90. https://doi.org/10.1016/j.surfin.2018.03.003

19. Maleki E, Unal O (2020) Optimization of shot peening effective parameters on surface hardness improvement. Met Mater Int 1–13. https://doi.org/10.1007/s12540-020-00758-x

20. Maleki E, Unal O, Amanov A (2018) Novel experimental methods for the determination of the boundaries between conventional, severe and over shot peening processes. Surf Interfaces 13:233–254. https://doi.org/10.1016/j.surfin.2018.09.003

21. Mohamed ALMO, Farhat Z, Warkentin A, Gillis J (2020) Effect of a moving automated shot peening and peening parameters on surface integrity of Low carbon steel. J Mater Process Technol 227:116399. https://doi.org/10.1016/j.jmatprotec.2019.116399

22. Wu J, Liu H, Wei P, Zhu C, Lin Q (2020) Effect of shot peening coverage on hardness, residual stress and surface morphology of carburized rollers. Surf Coat Technol 384:125273. https://doi.org/10.1016/j.surfcoat.2019.125273

23. Liu H, Wei Y, Tan CKI, Ardi DT, Tan DC, Lee CJJ (2020) XRD and EBSD studies of severe shot peening induced martensite transformation and grain refinements in austenitic stainless steel. Mater Charact 168:110574. https://doi.org/10.1016/j.matchar.2020.110574

24. Yang S, Zeng W, Yang J (2020) Characterization of shot peening properties and modelling on the fatigue performance of 304 austenitic stainless steel. Int J Fatigue 137:105621. https://doi.org/10.1016/j.ijfatigue.2020.105621

25. Chen M, Xing S, Liu H, Jiang C, Zhan K, Ji V (2020) Determination of surface mechanical property and residual stress stability for shot-peened SAF2507 duplex stainless steel by in situ X-ray diffraction stress analysis. J Mater Res Technol 9(4):7644–7654. https://doi.org/10.1016/j.jmrt.2020.05.028

26. Maleki E, Unal O, Kashyzadeh KR (2019) Efficiency analysis of shot peening parameters on variations of hardness, grain size and residual stress via taguchi approach. Met Mater Int 25(6):1436–1447. https://doi.org/10.1007/s12540-019-00290-7

27. Su N, Chen M, Xie L, Shi W, Luo F (2020) Dynamic characterization of Ti-4Al-1.5 Mn titanium alloy and a simplified approach for shot peening simulation. Int J Adv Des Manuf Technol 111(9):2733–2747. https://doi.org/10.1007/s00170-020-06299-2

28. Lin Q, Liu H, Zhu C, Parker RG (2019) Investigation on the effect of shot peening coverage on the surface integrity. Appl Surf Sci 489:66–72. https://doi.org/10.1016/j.apsusc.2019.05.281

29. Xiao X, Tong X, Sun Y, Li Y, Wei SM, Gao G (2019) An analytical model for predicting peening stresses with general peening coverage. J Manuf Process 45:242–254. https://doi.org/10.1016/j.jmapro.2019.06.029

30. Liu X, Liu J, Zuo Z, Zhang H (2019) Numerical study on residual stress redistribution of shot-peened aluminum 7075-T6 under fretting loading. Int J Mech Sci 160:156–164. https://doi.org/10.1016/j.ijmecsci.2019.06.031

31. Gariépy A, Miao HY, Lévesque M (2017) Simulation of the shot peening process with variable shot diameters and impacting velocities. Adv Eng Softw 114:121–133. https://doi.org/10.1016/j.advengsoft.2017.06.011

32. Bagherifard S, Ghelichi R, Guagliano M (2012) Numerical and experimental analysis of surface roughness generated by shot peening. Appl Surf Sci 258(18):6831–6840. https://doi.org/10.1016/j.apsusc.2012.03.11

33. Maleki E, Farrahi GH, Kashyzadeh KR, Unal O, Gugaliano M, Bagherifard S (2020) Effects of conventional and severe shot peening on residual stress and fatigue strength of steel AISI 1060 and residual stress relaxation due to fatigue loading: experimental and numerical simulation. Met Mater Int 27:1–17. https://doi.org/10.1007/s12540-020-00890-8

34. Zhang YL, Lai FQ, Qu SG, Ji V, Liu HP, Li XQ (2020) Effect of shot peening on residual stress distribution and tribological behaviors of 17Cr2Ni2MoVNb steel. Surf Coat Technol 386:125497. https://doi.org/10.1016/j.surfcoat.2020.125497

35. Zhao C, Shi C, Wang Q, Zhao C, Gao YK, Yang QX (2020) Residual stress field of high-strength steel after shot peening by numerical simulation. J Mater Eng Perform 29(1):358–364. https://doi.org/10.1007/s11665-020-04567-6

36. Sherafatnia K, Farrahi GH, Mahmoudi AH (2018) Effect of initial surface treatment on shot peening residual stress field: analytical approach with experimental verification. Int J Mech Sci 137:171–181. https://doi.org/10.1016/j.ijmecsci.2018.01.022

37. Song Z, Komvopoulos K (2014) An elastic–plastic analysis of spherical indentation: constitutive equations for single-indentation unloading and development of plasticity due to repeated

indentation. Mech Mater 76:93–101. https://doi.org/10.1016/j.mechmat.2014.05.005

38. Kim T, Lee H, Hyun HC, Jung S (2013) Effects of Rayleigh damping, friction and rate-dependency on 3D residual stress simulation of angled shot peening. Mater Des 46:26–37. https://doi.org/10.1016/j.matdes.2012.09.030

39. Wang XL, Wang Z, Wu G, Gan J, Yang Y, Huang HM, He JX, Zhong HL (2019) Combining the finite element method and response surface methodology for optimization of shot peening parameters. Int J Fatigue 129:105231. https://doi.org/10.1016/j.ijfatigue.2019.105231

40. Ghasemi A, Hassani-Gangaraj SM, Mahmoudi AH, Farrahi GH, Guagliano M (2016) Shot peening coverage effect on residual stress profile by FE random impact analysis. Surf Eng 32(11):861–870. https://doi.org/10.1080/02670844.2016.1192336

41. Xiao X, Tong X, Gao G, Zhao R, Liu Y, Li Y (2018) Estimation of peening effects of random and regular peening patterns. J Mater Process Technol 254:13–24. https://doi.org/10.1016/j.jmatprotec.2017.11.018

42. Wang C, Wang L, Wang XG, Xu YJ (2018) Numerical study of grain refinement induced by severe shot peening. Int J Mech Sci 146:280–294. https://doi.org/10.1016/j.ijmecsci.2018.08.005

43. Wang C, Hu JC, Gu ZB, Xu YJ, Wang XG (2017) Simulation on residual stress of shot peening based on a symmetrical cell model Chin. Aust J Mech Eng 30(2):344–351. https://doi.org/10.1007/s10033-017-0084-6

44. Kim T, Lee H, Jung S, Lee JH (2012) A 3D FE model with plastic shot for evaluation of equi-biaxial peening residual stress due to multi-impacts. Surf Coat Technol 206(13):3125–3136. https://doi.org/10.1016/j.surfcoat.2011.12.042

45. Wang C, Wang CL, Wang L, Lai YB, Li K, Zhou YJ (2020) A dislocation density–based comparative study of grain refinement, residual stresses, and surface roughness induced by shot peening and surface mechanical attrition treatment. Int J Adv Manuf Technol 108:505–525. https://doi.org/10.1007/s00170-020-05413-8

46. Wei Q, Wu WX, He W, Zhu JG, Zhang J (2020) 3D finite element simulation of shot peening using a sequential model with multiple-shot impacts. Int J Comp Meth-Sing 17(03):1850137. https://doi.org/10.1142/S0219876218501372

47. Miao HY, Larose S, Perron C, Lévesque M (2009) On the potential applications of a 3D random finite element model for the simulation of shot peening. Adv Eng Softw 40(10):1023–1038. https://doi.org/10.1016/j.advengsoft.2009.03.013

48. Rougier E, Munjiza A, Lei Z, Chau VT, Knight EE, Hunter A, Srinivasan G (2020) The combined plastic and discrete fracture deformation framework for finite-discrete element methods. Int J Numer Methods Eng 121(5):1020–1035. https://doi.org/10.1002/nme.6255

49. Gao W, Zang M, Xu W (2014) An approach to freely combining 3D discrete and finite element methods. Int J Comp Meth-Sing 11(01):1350051. https://doi.org/10.1142/S0219876213500515

50. Chung YC, Ooi JY (2012) Linking of discrete element modelling with finite element analysis for analysing structures in contact with particulate solid. Powder Technol 217:107–120. https://doi.org/10.1016/j.powtec.2011.10.016

51. Hong T, Ooi SB (2008) A numerical simulation to relate the shot peening parameters to the induced residual stresses. Eng Fail Anal 15(8):1097–1110. https://doi.org/10.1016/j.engfailanal.2007.11.017

52. Jebahi M, Gakwaya A, Lévesque J, Mechri O, Ba K (2016) Robust methodology to simulate real shot peening process using discrete-continuum coupling method. Int J Mech Sci 107:21–33. https://doi.org/10.1016/j.ijmecsci.2016.01.005

53. Tu F, Delbergue D, Klotz T, Bag A, Miao H, Bianc'hetti C, Brochu M, Bocher P, Levesque M (2018) Discrete element-periodic cell

coupling model and investigations on shot stream expansion, Almen intensities and target materials. Int J Mech Sci 145:353–366. https://doi.org/10.1016/j.ijmecsci.2018.06.023

54. Zhang J, Lu S, Wu T, Zhou Z, Zhang W (2018) An evaluation on SP surface property by means of combined FEM-DEM shot dynamics simulation. Adv Eng Softw 115:283–296. https://doi.org/10.1016/j.advengsoft.2017.10.001

55. Ahmad AS, Wu Y, Gong H (2020) Coupled finite and discrete element shot peening simulation based on Johnson–Cook material model. Proc Inst Mech Eng Part L 234(7):974–987. https://doi.org/10.1177/1464420720921211

56. Marini M, Piona F, Fontanari V, Bandini M, Benedetti M (2020) A new challenge in the DEM/FEM simulation of the shot peening process: The residual stress field at a sharp edge. Int J Mech Sci 169:105327. https://doi.org/10.1016/j.ijmecsci.2019.105327

57. Hu YZ, Tonder K (1992) Simulation of 3-D random rough surface by 2-D digital filter and Fourier analysis. Int J Mach Tool Manu 32(1-2):83–90. https://doi.org/10.1016/0890-6955(92)90064-n

58. Wu G, Wang Z, Gan J, Yang Y, Meng QS, Wei S, Huang HM (2019) FE analysis of shot-peening-induced residual stresses of AISI 304 stainless steel by considering mesh density and friction coefficient. Surf Eng 35(3):242–254. https://doi.org/10.1080/02670844.2018.1470817

59. Bagherifard S, Ghelichi R, Guagliano M (2014) Mesh sensitivity assessment of shot peening finite element simulation aimed at surface grain refinement. Surf Coat Technol 243:58–64. https://doi.org/10.1016/j.surfcoat.2012.04.002

60. Karpat Y (2011) Temperature dependent flow softening of titanium alloy Ti6Al4V: an investigation using finite element simulation of machining. J Mater Process Technol 211(4):737–749. https://doi.org/10.1016/j.jmatprotec.2010.12.008

61. Xie L, Zhang J, Xiong C, Wu L, Jiang C, Lu W (2012) Investigation on experiments and numerical modelling of the residual stress distribution in deformed surface layer of Ti-6Al-4V after shot peening. Mater Des 41:314–318. https://doi.org/10.1016/j.matdes.2012.05.024

62. Yin XN (2015) Surface integrity study on shot peened Ti-6Al-4V titanium alloy, MD-thesis. Dalian University of Technology

63. Klemenz M (2009) Anwendung der simulation der RandschichtausbildungbeimKugelstrahlen auf die Abschätzung der SchwingfestigkeitgekerbterBauteile. PhD-thesis. Shaker, Aachen: Universität Karlsruhe